Available online at www.sciencedirect.com
SCIENCE DIRECT
Catalysis Today 116 (2006) 281–288
CATALYSIS TODAY
www.elsevier.com/locate/cattod

Autothermal catalytic pyrolysis of methane as a new route to hydrogen production with reduced CO_2 emissions

Nazim Muradov *, Franklyn Smith, Cunping Huang, Ali T-Raissi

Florida Solar Energy Center, University of Central Florida, Cocoa, FL 32922, USA

Available online 27 June 2006

Abstract

Hydrogen production plants are among major sources of CO_2 emissions into the atmosphere. The objective of this paper is to explore new routes to hydrogen production from natural gas (or methane) with drastically reduced CO_2 emissions. One approach analyzed in this paper is based on thermocatalytic decomposition (or pyrolysis) of methane into hydrogen gas and elemental carbon over carbon-based catalysts. Several heat input options to the endothermic process are discussed in the paper. The authors conduct thermodynamic analysis of methane decomposition in the presence of small amounts of oxygen in an autothermal (or thermo-neutral) regime using AspenPlus™ chemical process simulator. Methane conversion, products yield, effluent gas composition, process enthalpy flows as a function of temperature, pressure and O_2/CH_4 ratio has been determined. CO_2 emissions (per m^3 of H_2 produced) from the process could potentially be a factor of 3–5 less than from conventional hydrogen production processes. Oxygen-assisted decomposition of methane over activated carbon (AC) and AC-supported iron catalysts over wide range of temperatures and O_2/CH_4 ratios was experimentally verified. Problems associated with the catalyst deactivation and the effect of iron doping on the catalyst stability are discussed.

Keywords: Hydrogen; Carbon; Methane; Catalyst; Autothermal pyrolysis

1. Introduction

Presently, most of the industrial hydrogen production is based on steam methane reforming (SMR) process, which is a source of significant CO_2 emissions into the atmosphere. It was estimated that the global warming potential of hydrogen production via SMR process is 13.7 kg CO_2 (equiv.)/kg of net hydrogen produced [1]. Catalytic decomposition of methane has recently attracted the attention of researchers for it could potentially lead to the development of CO_2-free hydrogen production process [2–4].

$$CH_4 \rightarrow C + 2H_2 \quad \Delta H^\circ = 75.6\,\text{kJ/mole} \tag{1}$$

Due to very strong C–H bonds in methane molecule its thermal (non-catalytic) decomposition occurs at very high temperatures (>1200 °C). Various transition metal catalysts (e.g., Ni, Fe, Co) have been used to reduce the maximum temperature of methane thermal decomposition [5–7]. The major problems associated with the use of metal catalysts relate to their rapid deactivation (due to blocking of surface active sites by carbon deposits) and difficulties involving metal–carbon separation. The use of carbon-based catalysts offers distinct advantages over metal catalysts due to their availability, durability and low cost. In contrast to metal-based catalysts, carbon catalysts are sulfur and temperature resistant and do not require their separation from the carbon-product. The technical feasibility of using carbon materials as catalysts for methane decomposition reaction is discussed in several publications (e.g. [7,8]). The data on catalytic activity of a variety of carbon materials of different origin and structure, including a wide range of activated carbons (AC) and carbon blacks (CB), toward methane decomposition reaction has been reported before [8–10]. The major factors determining the activity and stability of carbon catalysts for methane decomposition reaction, as well as issues related to the catalyst deactivation and regeneration were recently discussed [11,12]. The objective of this paper is to analyze and experimentally validate a novel technological approach to environmentally friendly production of hydrogen from natural gas (NG), in particular, via catalytic autothermal pyrolysis of methane.

* Corresponding author. Tel.: +1 321 638 1448; fax: +1 321 504 3438.
E-mail address: muradov@fsec.ucf.edu (N. Muradov).

0920-5861/$ – see front matter © 2006 Elsevier B.V. All rights reserved.
doi:10.1016/j.cattod.2006.05.070

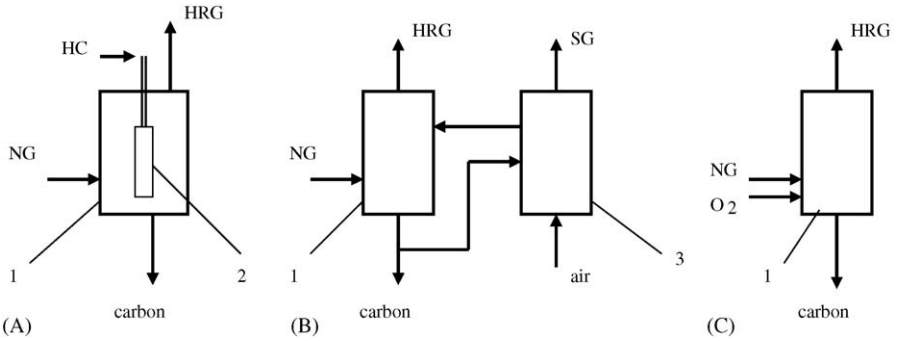

Fig. 1. Heat input options: internal (A), external (B) and thermo-neutral (C). Three process heat input options for thermocatalytic decomposition of methane. NG, natural gas; HRG, hydrogen-rich gas; SG, stack gases; HC, heat carrier. 1, methane decomposition reactor, 2, reactor heater, 3, catalyst particles heater.

2. Heat input options for methane catalytic decomposition

Methane decomposition is a moderately endothermic reaction: the thermal energy requirement per mole of hydrogen produced is only 37.8 kJ/mole H_2 compared to 63 kJ/mole H_2 for SMR. Less than 10% of the methane heating value is needed to drive the endothermic process. The amount of CO_2 emissions from the process could potentially be as low as 0.05 mole CO_2/mole H_2 (if methane is used as a process fuel), compared to 0.43 mole CO_2/mole H_2 for SMR [3]. CO_2 emissions could potentially be eliminated, if a part of hydrogen product (theoretically, 16%) is combusted to produce process heat.

Fig. 1(A–C) illustrates three options for supplying heat to the endothermic methane decomposition process. According to the option (A) the heat source is located inside the reaction zone. It could be a heat pipe, a heat exchanger or a tubular catalytic burner that uses NG or a portion of hydrogen product as a fuel. For example, the sodium heat pipes have been demonstrated for efficient heat transfer in methane steam reformers [13]. In concept (B) the process heat is introduced to the reactor by externally heated catalyst particles similar to fluid catalytic cracking or fluid coking processes widely used in refineries. The process employs two fluid–solid vessels: a reactor and a heater with catalyst particles circulating between the vessels in a fluidized state. This technological concept has been described in our earlier publications (e.g. [14]) and will not be discussed here. According to the concept (C) a relatively small amount of oxygen is fed into the reactor along with the methane feedstock to generate heat required to accomplish the endothermic methane decomposition reaction. This approach may appear similar to the well-known partial oxidation (PO_x) process. However, there is a difference between the two processes. In particular, PO_x process is intended for complete conversion of methane into synthesis gas and, therefore, it requires relatively large amount of oxygen (O_2:CH_4 = 0.5 mole/mole). In contrast, the objective of oxygen-assisted methane decomposition is to maximize the yields of both hydrogen and carbon products by introducing oxygen in an amount just enough to sustain the endothermic methane decomposition reaction. We refer to this process as the autothermal pyrolysis (ATP) since it involves the combination of endothermic (methane decomposition) and exothermic (methane combustion) processes in one reactor (i.e., the process operates in a thermo-neutral regime). It is evident that ATP process would produce much less CO_2 emissions than PO_x or SMR since it uses less oxidant. Advantageously, in the ATP process most of the feedstock carbon ends up in the form of value-added carbon product rather than CO_2.

One should also distinguish ATP from a number of other processes involving oxidative conversion of methane, e.g., partial combustion of methane to carbon or acetylene, oxidative coupling of methane to ethylene, etc. Fig. 2 depicts the data on the standard enthalpies of different methane conversion processes as a function of the O_2/CH_4 molar ratio. Hereafter, O_2/CH_4 molar ratio will be designated as χ (thus, $\chi = O_2/CH_4$, and the corresponding gaseous mixture is presented as $CH_4 + \chi O_2$). It can be seen that the process enthalpies decrease almost linearly with χ. Anaerobic decomposition of methane (at $\chi = 0$) and complete combustion of methane (at $\chi = 2$) noted by the points lying on the opposite ends of the plot.

In the following sections we explore some process development issues related to the production of hydrogen and carbon by ATP of methane. In particular, we conduct thermodynamic analysis of methane thermal decomposition with temperature, pressure and O_2/CH_4 ratio as variables. Experimental verification of ATP of methane in a wide range of temperatures and χ over carbon-based catalysts is also provided.

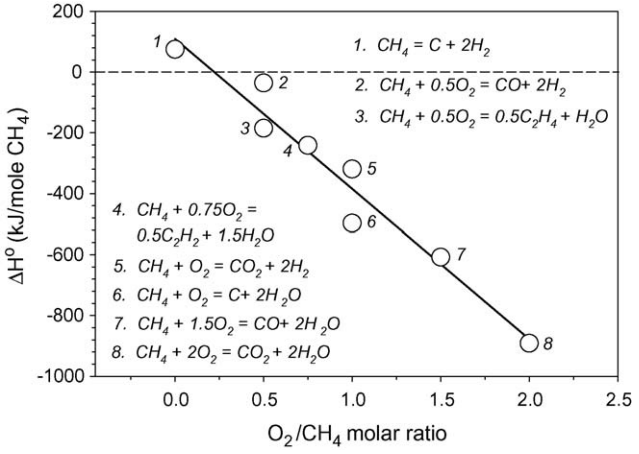

Fig. 2. Standard enthalpies of different methane conversion processes vs. O_2/CH_4 ratio.

3. Thermodynamic analysis of autothermal pyrolysis of methane

AspenPlus™ chemical process simulator was used to calculate the thermodynamic equilibria of CH_4–χO_2 system. The reactions involved were modeled using a Gibbs reactor to minimize the free energy in order to calculate thermodynamic parameters of the process at the given operating conditions. Input parameters were: inlet pressure and temperature, reactor temperature and pressure, and χ. Peng-Robinson property package was used in the reaction equilibrium calculations. Methane conversion, products yields, pyrolysis gas composition, process enthalpy, entropy and Gibbs free energy flows were determined as a function of temperature, pressure and χ. A range of temperatures, pressures and O_2/CH_4 ratios of, respectively, $T = 300$–1200 °C, $P = 0.1$–2.5 MPa and $\chi = 0$–1.5 was chosen for the thermodynamic analysis of the process.

Fig. 3 depicts the three-dimensional plots of methane conversion as a function of temperature and χ at two pressures: $P = 0.2$ and 2.5 MPa. It is evident from Fig. 3 that at both pressures methane conversion increases drastically with the increase in both T and χ. For example, at $P = 0.2$ MPa, $T = 850$ °C and relatively low O_2/CH_4 ratios ($\chi \leq 0.2$) methane conversion approaches 90%. However, at $P = 2.5$ MPa (with temperature and χ remaining the same), methane conversion is

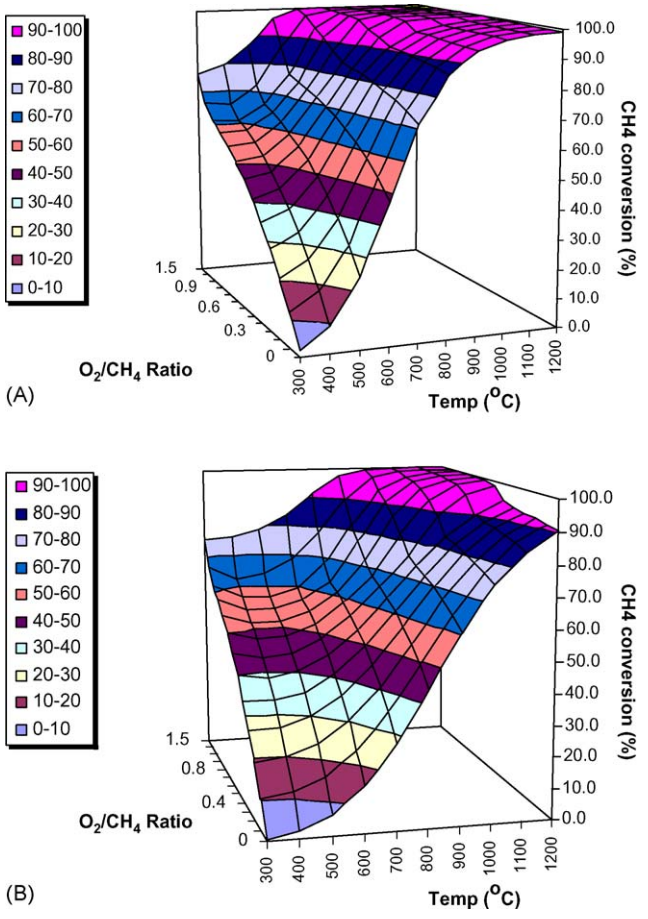

Fig. 3. Methane conversion as a function of temperature and O_2/CH_4 ratio at $P = 0.2$ MPa (A) and 2.5 MPa (B).

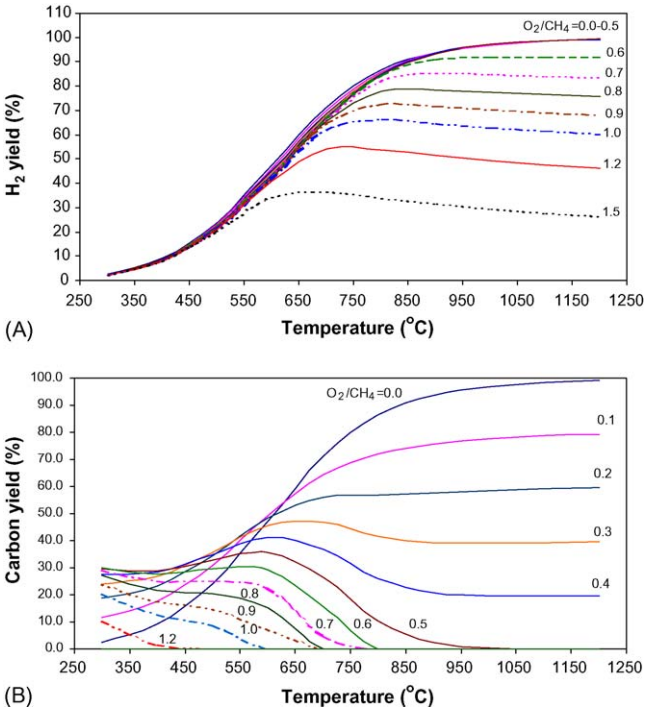

Fig. 4. Temperature dependence of H_2 (A) and carbon (B) yields with O_2/CH_4 ratio as a variable ($P = 0.2$ MPa).

below 60%, which indicates that the process is not thermodynamically favored at high pressures.

Fig. 4 illustrates the effect of temperature on the yield of hydrogen and carbon with χ as a variable and $P = 0.2$ MPa. Results of Fig. 4 indicate that the hydrogen yield is not appreciably affected by the change in O_2/CH_4 ratio within the range of $0 < \chi < 0.5$. However, at $\chi > 0.5$ hydrogen yield drops markedly, which is accompanied with an increase in the yield of water produced. In contrast, carbon yield is quite sensitive to even slight increase in the value of χ in the entire range of O_2/CH_4 ratios. At $\chi > 0.6$ carbon is not present among the reaction products at temperatures above 800 °C.

Fig. 5 depicts the total enthalpy flow within the reactor as a function of temperature and χ. The total rate of enthalpy flow was calculated as a sum of the rates of outlet enthalpies of all products minus sum of the rates of inlet enthalpies of CH_4–χO_2 mixtures. A negative enthalpy flow indicates that at given χ, T and P, the process generates heat, which would require its removal from the reactor. On the other hand, positive enthalpy flow implies that at given conditions a certain amount of thermal energy has to be supplied to the reactor in order to accomplish methane decomposition. Results of Fig. 5 show that for the practical range of temperatures (600–900 °C) and pressures ($P = 0.1$–2.5 MPa), the enthalpy flow is close to zero (which corresponds to autothermal or thermo-neutral regime) at O_2/CH_4 ratio of $\chi \approx 0.2$.

Fig. 6 demonstrates molar fraction of methane conversion products as a function of temperature at atmospheric pressure and $\chi \approx 0.2$. It can be seen that within the temperature range of 500–850 °C hydrogen and carbon are the main reaction products with the yield of CO increasing steadily and

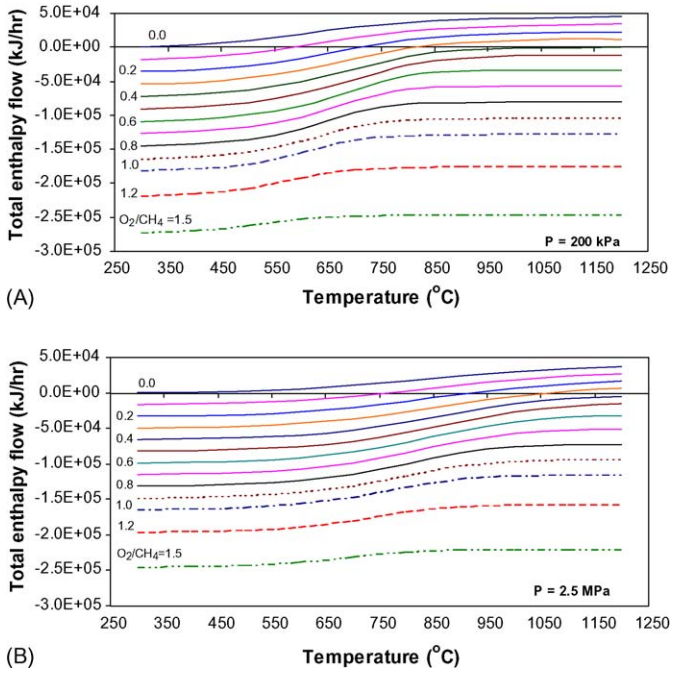

Fig. 5. Total enthalpy flow for methane decomposition reaction as a function of temperature at $P = 0.2$ MPa (A) and 2.5 MPa (B). Enthalpy flow relates to 0.45 kmole/h of CH_4–χO_2 mixture.

approaching a plateau. At $T > 850$ °C, the molar fractions of the methane decomposition/oxidation products (H_2, C and CO) are nearly independent of the reactor temperatures. At these conditions (i.e., $T \geq 850$ °C, $P = 0.1$ MPa and $\chi \approx 0.2$), the distribution of the products of methane ATP is consistent with the following stoichiometric equation:

$$CH_4 + 0.2O_2 \rightarrow 2H_2 + 0.6C + 0.4CO \quad (2)$$

Thus, the equilibrium composition of the gaseous products of ATP of methane at $P = 0.1$ MPa, $\chi \approx 0.2$ and $T \geq 850$ °C corresponds to the following mixture: $[H_2] \approx 83$, $[CO] \approx 17$ vol.%. It is noteworthy that the concentration of hydrogen (83 vol.%) is significantly higher than that produced by SMR ($[H_2] \approx 52$ vol.% in the row gas and 72 vol.% in the dry gas [15]) and PO_x ($[H_2] \approx 66$ vol.% using oxygen and 35 vol.% for air) processes.

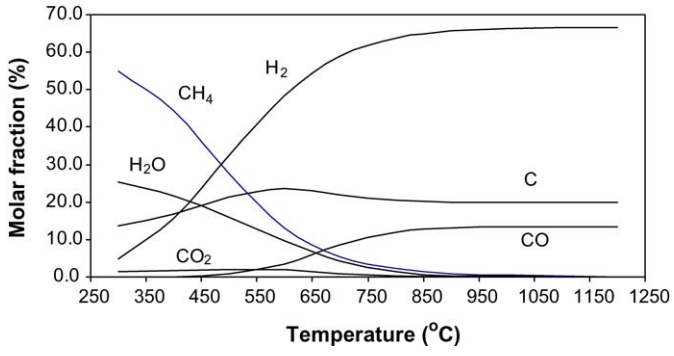

Fig. 6. Molar fraction of methane conversion products as a function of temperature at $P = 0.1$ MPa and $\chi \approx 0.2$.

4. Engineering considerations of hydrogen production via ATP of NG

The issues related to the selection of a reactor suitable for methane decomposition with continuous withdrawal of carbon product were described in our earlier publication [14]. Several types of reactors, including tubular, fluid wall, spouted and fluidized bed reactors were evaluated, and the latter was selected as the most promising for a large scale operation. In a fluidized bed reactor (FBR) the bed of fine catalyst particles behaves as a well-mixed body of liquid giving rise to high particle-to-gas heat and mass transfer.

Fig. 7 depicts a simplified block-diagram of the ATP process with NG as a feedstock. The presence of oxygen in the feedstock results in the production of CO byproduct (see Eq. (2)) that would require the addition of water-gas shift (WGS) reactor(s) 4 to the process train. However, due to relatively low concentration of CO in the gaseous product (~17 vol.%) the WGS unit in the ATP process would be much smaller than that in conventional SMR and PO_x processes. In the final stage of the process, high-purity hydrogen (>99.99 vol.%) could be recovered from H_2–CO_2 gaseous mixture (or H_2–CH_4–CO_2 mixture if a portion of the methane remains unconverted) using a gas separation unit 5 (e.g., pressure-swing adsorption, H_2-permeable membrane, cryogenic separation unit). Unconverted methane is separated from the gaseous mixture and recycled to the FBR 1.

If a metal catalyst is used in the process, it is to be separated from the carbon product in a catalyst-carbon separation unit 6, reactivated in a regenerator 7 and recycled to the FBR. In case of carbon-based catalysts, carbon-product will be deposited on the surface of the carbon-catalyst forming one product (i.e., no need for the catalyst-carbon separation). A portion of carbon particles is withdrawn from the process as a final product; this allows keeping the carbon inventory steady and controlling carbon particle size. Within the FBR, the coarser carbon particles (grown by carbon lay down) are converted to smaller

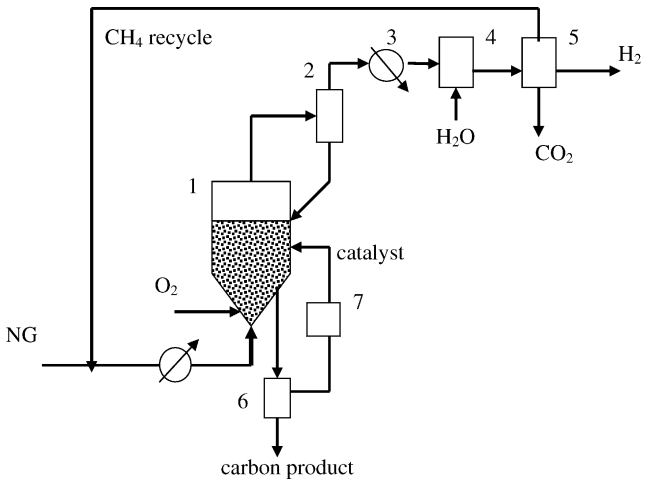

Fig. 7. Schematic diagram of hydrogen and carbon production via catalytic autothermal pyrolysis of natural gas. 1, fluidized bed reactor, 2, cyclone, 3, heat exchanger, 4, water gas shift reactor, 5, gas separation unit, 6, carbon separation unit, 7, catalyst regeneration unit.

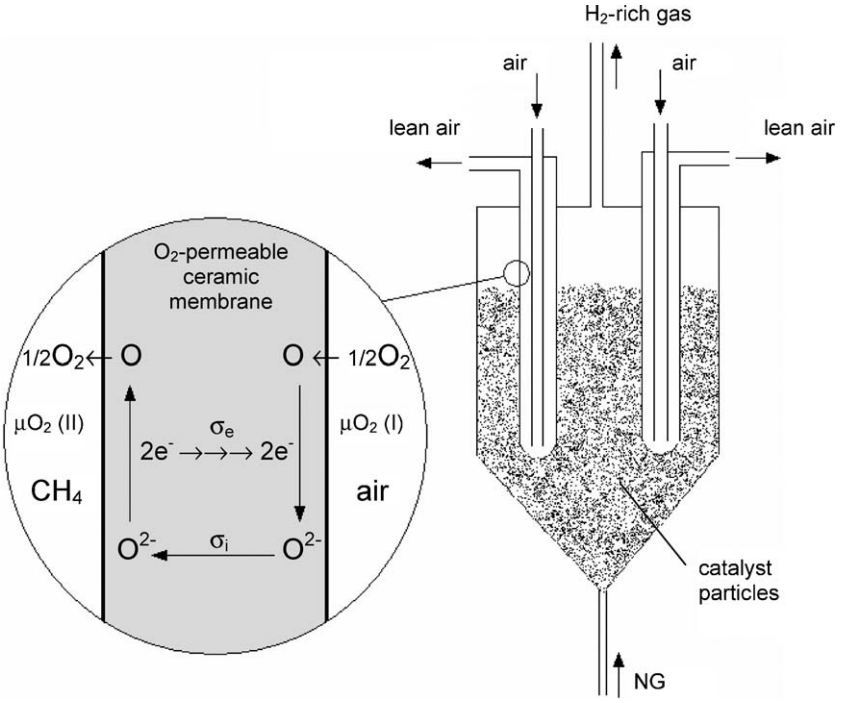

Fig. 8. Schematics of ATP fluidized bed reactor equipped with a tubular oxygen-permeable ceramic membrane. A blow-up section of the figure shows the detail of the ceramic membrane wall (explaining the mechanism of oxygen permeation across the membrane). μ is the chemical potential of oxygen. σ_i and σ_e are the ionic and electronic components of the conductivity, respectively.

seed carbon particles using the attriters located at the bottom of the FBR (similar to fluid coking process [16]). Carbon is a valuable byproduct of the process and, if marketed, it could significantly reduce the cost of hydrogen production.

Due to relatively low endothermicity of the methane decomposition reaction and the elimination (or reduction in size) of energy-intensive steam production and gas conditioning stages, the CO_2 emission from the ATP could potentially be much less than that from conventional processes. It is estimated that CO_2 emissions from ATP process could be as low as 0.17 m^3/m^3 H_2, which is almost one third of that produced by the SMR process (per m^3 H_2) (or one fifth of that from the steam-oxygen gasification of coal). On the down side, ATP process requires an expensive oxygen production unit, which would add to the cost of hydrogen production. The usage of air instead of oxygen may result in a larger and more expensive gas separation unit. Therefore, alternative means of introducing oxygen into the fluidized bed reactor have to be considered. One promising approach involves the use of ceramic oxygen-permeable membranes.

It is well known that dense ceramic membranes made of the mixture of ionic and electron conductors are permeable to oxygen at elevated temperatures. For example, perovskite-type oxides (e.g., La–Sr–Fe–Co, Sr–Fe–Co and Ba–Sr–Co–Fe based mixed oxide systems) are good oxygen-permeable ceramics. Extensive research has been carried out on the application of ceramic O_2-permeable membranes to PO_x and other processes requiring pure oxygen. For example, a membrane reactor containing O_2-permeable ceramic membrane made of $Ba_{0.5}Sr_{0.5}Co_{0.8}Fe_{0.2}O_{3-\delta}$ has been successfully applied to PO_x of methane at 900 °C [17]. Fig. 8 depicts a conceptual design of an ATP fluidized bed reactor equipped with a tubular oxygen-permeable dense ceramic membrane. A detail of the ceramic membrane wall depicting the mechanism of oxygen permeation through the membrane is given on the left side of Fig. 8. The gradient of oxygen pressure (or its chemical potential, μ) is the driving force for oxygen transport across the ceramic membrane. Advantageously, the O_2-permeable ceramic membranes operate efficiently at the same temperature range as the ATP process (i.e., 800–900 °C). Stoichiometrically, ATP requires 2.5 times less oxygen per mole of methane than PO_x. Consequently, oxygen flux requirements for a membrane in the case of ATP process would be much less demanding than the PO_x process, with potentially important practical implications.

5. Experimental verification of ATP of methane

We conducted a series of proof-of-the-concept experiments on oxygen-assisted catalytic decomposition of methane. Fig. 9 depicts distribution of methane decomposition/oxidation products (in molar %) as a function of O_2/CH_4 molar ratio at 900 °C in the presence of AC (lignite) as a catalyst. Hydrogen, carbon and CO are the main products of methane conversion. Minute amounts of ethylene (<0.1 mol.%) were also detected among the reaction products. As expected, hydrogen and carbon yields decrease and H_2O, CO_x yields increase with the increase in O_2/CH_4 ratio in the entire range of χ (due to methane partial combustion). Interestingly, ethylene yield first increases reaching maximum at $\chi = 0.25$ and then

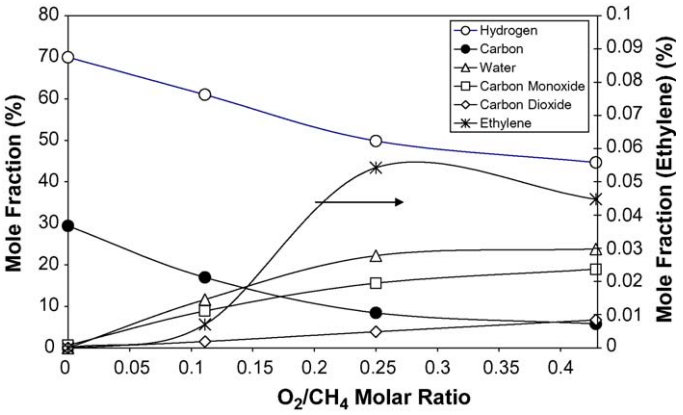

Fig. 9. Molar fraction of products of methane decomposition as a function of O_2/CH_4 ratio. $T = 900$ °C, $P = 0.1$ MPa.

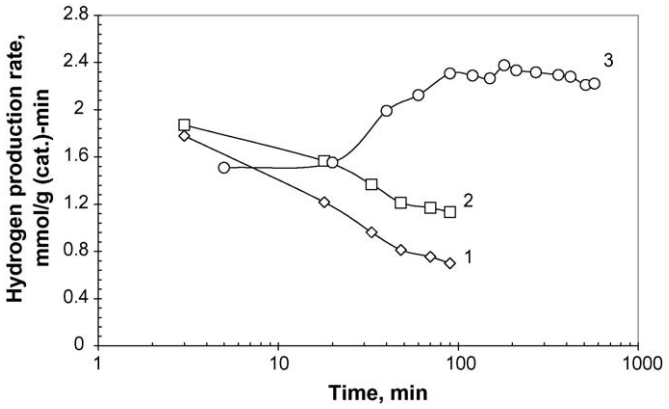

Fig. 11. Time dependence of hydrogen production rate during thermocatalytic decomposition of methane over different catalyst at 900 °C. 1, AC-lignite, no O_2 present, 2, AC-lignite, $O_2/CH_4 = 0.2$ (molar), 3, Fe (10 wt.%)/AC-lignite, $O_2/CH_4 = 0.2$.

decreases. Fig. 10 illustrates the temperature dependence of the products yields (in mol.%) at $\chi = 0.2$ using AC (lignite). It is evident that in the temperature range of 850–1000 °C, the CO_x yields remain almost independent of temperature, and the yield of carbon and, particularly, hydrogen steadily increases. The yields of water and C_2 hydrocarbons significantly drop at the same range of temperatures. X-ray diffraction (XRD) analysis of the carbons produced by methane decomposition over AC (produced from coconut, lignite, peat) catalysts revealed that their crystallographic structure is consistent with the disordered (or turbostratic) carbon structure.

Fig. 11 depicts the time dependence of hydrogen production rate (in mmole H_2 per gram of catalyst per minute) at 900 °C for three different cases (in semi-log coordinates). The first case (curve 1) relates to anaerobic methane decomposition (i.e., $\chi = 0$) over AC (lignite). The second curve represents oxygen-assisted ($\chi = 0.2$) methane decomposition over the same AC catalyst. It is clear that the addition of oxygen to the system has noticeably slowed down the rate of catalyst deactivation. Since main factors contributing to carbon catalyst deactivation relate to the deposition of catalytically inactive carbon species and the loss of surface area [11], it can be hypothesized that the presence of small amounts of oxygen promotes methane decomposition by creating more active sites on the catalyst surface and maintaining relatively high surface area. Indeed, BET surface area measurements of carbon samples after the AC (lignite)-catalyzed methane decomposition experiments have shown that the surface area of the carbon product formed in the presence of oxygen ($\chi = 0.2$) is somewhat greater than that of the carbon produced under anaerobic conditions. Curve 3 corresponds to oxygen-assisted ($\chi = 0.2$) methane decomposition in the presence of AC (lignite)-supported iron (10 wt.%) catalyst. There is an initial induction period on the kinetic curve, which corresponds to the reduction of iron oxides to the active metallic form of the catalyst. This was followed by relatively steady methane decomposition process (for about 10 h) with the formation of the same product species as in the case of AC catalyst. It is evident that doping carbon catalyst with iron significantly improved the catalyst activity and stability. The positive effect of iron on the reaction is no surprise: high catalytic activity of iron in methane

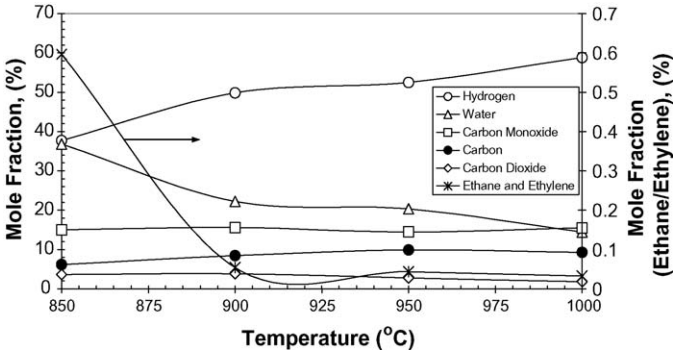

Fig. 10. Experimentally determined temperature dependence of the molar fraction of methane decomposition products. $O_2/CH_4 = 0.2$ (molar), $P = 0.1$ MPa.

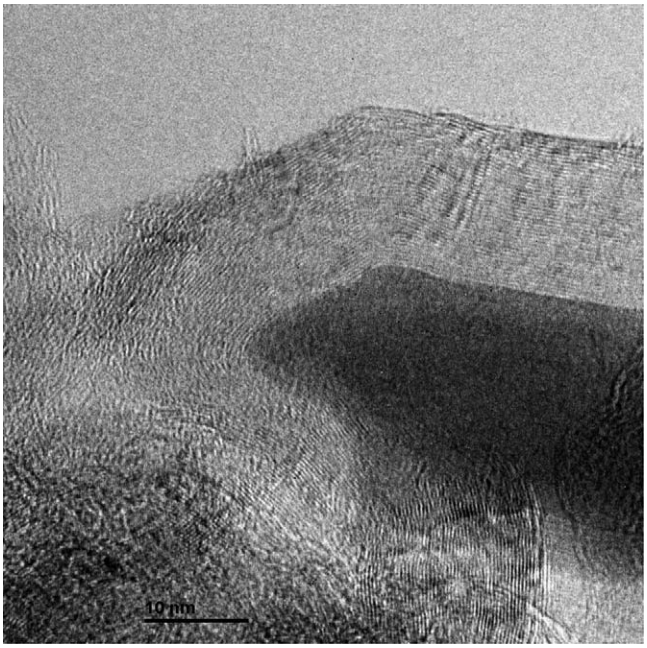

Fig. 12. TEM image of Fe (10 wt.%)/AC-lignite catalyst with carbon deposits produced by methane decomposition (900 °C) in the absence of oxygen.

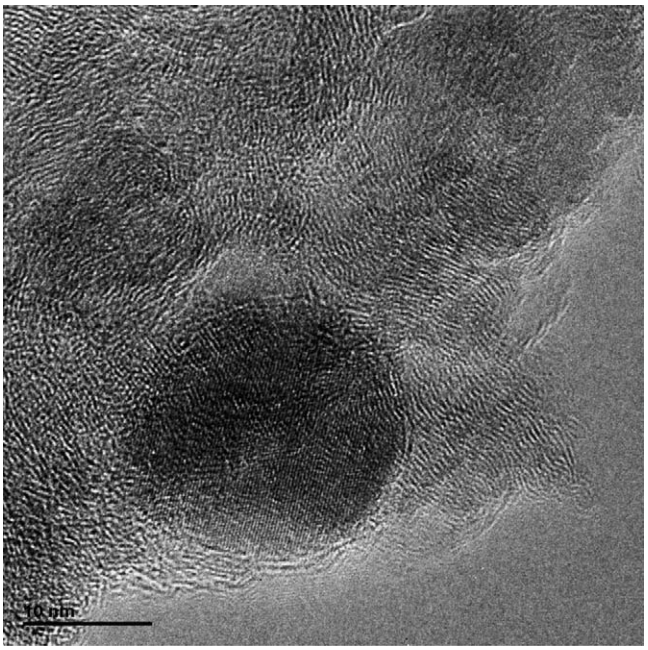

Fig. 13. TEM image of Fe (10 wt.%)/AC-lignite catalyst with carbon deposits produced by methane decomposition (900 °C) in the presence of oxygen (O_2/CH_4 = 0.2).

decomposition reaction is well-documented (e.g., [5,7]). On the other hand, alumina- and silica-supported iron-based catalysts are known for their rapid deactivation due to blocking of active sites by carbon deposits (e.g. [5]). Thus, the combination of iron catalyst with a carbon support ensures better performance through some synergistic action, the nature of which is yet unknown.

Figs. 12 and 13 depict typical high-resolution transmission electron microscopic (TEM) images of carbon produced by methane decomposition over Fe (10 wt.%)/AC-lignite catalysts under anaerobic condition and in the presence of oxygen (χ = 0.2), respectively. It can be seen that in the former case the iron particle (the dark spot) is completely covered by several (about 40–50) layers of carbon, which is implicated in the deactivation of the catalyst. Fig. 13 shows the TEM image of the nano-size iron particle (~20 nm) that is only partially coated with carbon layers; the lower part of the particle has only two carbon layers and could be still catalytically active toward methane decomposition. It is plausible that in the presence of oxygen the iron particle partially catalyzes the oxidation of carbon layers, thus, preventing a buildup of large carbon deposits on its surface (at least, on some parts of the surface). This effect could potentially reduce the rate of catalyst deactivation and result in a better performance (compared to the same catalyst working under anaerobic conditions). It is also noteworthy that carbon layers around the iron particle are much less ordered compared to the carbon sample from the anaerobic experiment (see Fig. 12), where carbon layers almost perfectly organized themselves in a parallel pattern. Our earlier studies (e.g. [8]) indicated that disordered carbons (e.g., CB, AC) are catalytically more active for methane decomposition than ordered ones (e.g., graphite). Thus, the presence of disordered carbon species could be another important factor contributing to higher catalytic activity of the carbon-supported iron catalyst.

The comparison of thermodynamic equilibrium (Fig. 6) and experimentally determined (Fig. 10) data on products distribution reveals some agreements as well as disparities. In particular, it can be seen that the molar fractions of hydrogen in the products mix on both plots are in fairly good agreement (within less than 10% margin of error), whereas the molar distribution of other products is quite dissimilar. For example, thermodynamic equilibrium data indicate that carbon yield exceeds that of CO, whereas experimental results show an opposite trend (i.e., CO yield is greater than that of carbon). Moreover, at the temperatures above 850 °C the thermodynamic equilibrium values for CO_2 and H_2O are close to zero, which, apparently, is not in agreement with the experimentally determined values. Factors underlying these discrepancies are yet to be determined. One can speculate that the presence of relatively large quantities of carbon (which is both a catalyst and reaction product, at the same time) in the system may hinder formation of carbon and shift the equilibrium in favor of CO.

6. Experimental

Methane (99.99 vol.%) and oxygen (99.99 vol.%) (both from Air Products and Chemicals, Inc.) were used without further purification. Samples of activated carbons (lignite, peat and coconut) were obtained from Alfa Aesar and Barneby Sutcliffe and were used in the form of pellets (1–1.5 mm). Surface area of AC samples were (m^2/g): lignite, 650, peat, 900, coconut, 1150. Oxygen-assisted methane decomposition experiments were conducted using a quartz micro-reactor (inner diameter 8 mm) with a bed of a catalyst material (0.1 g). Carbon-supported iron (10 wt.% based on metallic iron) catalysts were prepared by the conventional soaking–drying technique using iron(III) nitrate followed by calcination of the catalyst at 650 °C for 2 h. All catalyst samples were dried (400 °C, 2 h) before the experiments in a stream of Ar to remove adsorbed water and pore-entrained air. The catalysts were weighed before and after experiment to determine the amount of carbon produced. The amount of water produced in the reaction was determined by measuring the weight gain of a bed of adsorbent pellets (Drierite) placed downstream the reactor during the experiment (the margin of error: 5%). The reactor was maintained at a constant temperature via a type K thermocouple connected to a Love Controls temperature controller. All experiments were conducted at atmospheric pressure. The residence time in the catalyst layer was in the order of 0.1 s. On-line analysis of the effluent gas (H_2, O_2, CO, CO_2, CH_4, C_2H_6, C_2H_4) was performed gas chromatographically (the combination of two SRI-8610A chromatographs with TCD, Ar-carrier gas, silica gel column and FID, He-carrier gas, HysepD$_b$ column). Analysis of carbon products was conducted by X-ray diffraction (XRD, Rigaku) and scanning (SEM, Jeol 6400F) and transmission (TEM, FEI Tecnai F30) electron microscopic methods.

7. Conclusion

Catalytic dissociation of hydrocarbons is a promising approach to fossil fuel-based hydrogen production without (or minimal) CO_2 emissions. Methane decomposition is a moderately endothermic reaction. Several technological approaches to the process heat supply including internal, external and autothermal (or thermo-neutral) options are discussed in this paper. The latter option offers certain advantages over other approaches due to its simplicity and versatility. Thermodynamic analysis (AspenPlus^{TM}) of methane decomposition reaction in the presence of oxygen indicated that at the practical range of temperatures (600–900 °C) and pressures (0.1–2.5 MPa) autothermal pyrolysis of methane could be accomplished at O_2/CH_4 molar ratio of about 0.2. ATP of methane was experimentally verified using activated carbon and iron-doped carbon catalysts. CO_2 emissions (per m^3 of H_2 produced) from the process could potentially be a factor of 3–5 less than from conventional hydrogen production processes. The technology could be suitable for environmentally friendly centralized and distributed production of hydrogen

Acknowledgements

This work was supported by the NASA Glenn Research Center under contract No. NAG32751. The authors thank Zia Rahman (MCF, UCF) for conducting TEM and SEM analysis of the carbon samples and Tim Smith (NASA-GRC) and Dr. David L. Block (FSEC).

References

[1] P. Spath, M. Mann; Technical Report NREL/TP-570-27637, NREL, 2000.
[2] N. Muradov, Int. J. Hydrogen Energy 18 (1993) 211.
[3] M. Steinberg, Int. J. Hydrogen Energy 24 (1990) 771.
[4] B. Gaudernack, S. Lynum, in: Proceedings of 11th World Hydrogen Energy Conference, Stuttgart, (1996), p. 511.
[5] M. Calahan, in: G. Sandstede (Ed.), From Electrocatalysis to Fuel Cells, Univ. Washington Press, Seattle, 1972, p. 189.
[6] N. Shah, D. Panjala, G. Huffman, Energy Fuels 15 (2001) 1528.
[7] N. Muradov, Energy Fuels 12 (1998) 41.
[8] N. Muradov, F. Smith, Catal. Commun. 2 (2001) 89.
[9] R. Moliner, I. Suelves, M. Lazaro, O. Moreno, Int. J. Hydrogen Energy 30 (2005) 293.
[10] M. Kim, E. Lee, J. Jun, S. Kong, G. Hun, B. Lee, K. Yoon, Int. J. Hydrogen Energy 29 (2004) 187.
[11] N. Muradov, F. Smith, A. T-Raissi, Catal. Today 102–103 (2005) 225.
[12] N. Muradov, F. Smith, in: M. Marini, G. Spazzafumo (Eds.), Hydrogen Power Theoretical and Engineering Solutions, SGEditoriali, Padova, Italy, 2003, pp. 87–95.
[13] J. Richardson, Proc. Natural Gas Conversion IV, vol. 107, Elsevier, Oxford, 1997.
[14] N. Muradov, Int. J. Hydrogen Energy 26 (2001) 1165.
[15] Ullmann's Encyclopedia of Industrial Chemistry, vol. A-13, VCH, 1985.
[16] S. Massenzio, Handbook of Synfuel Technology, McGraw Hill Book Company, NY, 1984, pp. 3–18.
[17] C. Chen, S. Feng, S. Ran, D. Zhu, W. Liu, H. Bouwmeester, Angew. Chem. Int. Ed. 42 (2003) 5196.